Direct measurement of the free-energy barrier to nucleation from the size distribution of dendritic crystallites in a-Si thin films

Hideya Kumomi*
Canon Inc., Research and Development Headquarters, 6770 Tamura, Hiratsuka, Kanagawa 254, Japan

Frank G. Shi
Chemical Engineering and Materials Science Department, University of California, Irvine, California 92717-2575
(Received 27 February 1995)

We introduce a method to determine the free-energy barrier to nucleation of crystallites, independent of any model for the nucleation free-energy barrier, and independent of the energy barrier to the growth. This model-independent method is developed based on the dynamic scaling of the cluster size distribution and other universal kinetics in the early stages of nucleation and growth. The method is applied to determine the free-energy barrier to nucleation of the amorphous-to-crystalline transformation in a-Si thin films. After considering the dendritic nature of Si crystallites, we obtain the free-energy barrier to nucleation $W_* \approx 2.15$–2.18 eV, the enthalpic (i.e., the activation energy) barrier $\Delta H_* = 1.32$ eV, and the entropic barrier $\Delta S_* = -9.57 \times 10^{-4}$ eV K^{-1}, within the temperature range of $T = 863$–893 K. The entropic contribution to W_* is found to be considerably large. We also show that the magnitude of the measured W_* could not be accounted for by the classical expression for the free-energy barrier with the previous suggested values for its parameters.

I. INTRODUCTION

Atoms of a disordered amorphous material always attempt to rearrange themselves into small and ordered clusters, because the free energy of the crystalline phase is lower than that of the amorphous one. Through random fluctuations, some clusters eventually become crystalline nuclei that initiate the amorphous-to-crystalline phase transformation. Thus, understanding the free-energy barrier to nucleation of crystallites, W_*, is a basic issue in materials physics. There are various classical and nonclassical models for W_*, but to our knowledge none of those models have been tested by a direct and model-independent experimental determination of W_*.[1] This is not surprising, because conventional methods employing Arrhenius plots do not measure the free-energy barrier, W_*, but the apparent activation energies, i.e., enthalpies.[2] Recently a model-independent method for determining W_* was introduced, which determines the free-energy barrier, W_*, using the ratio of the growth rate to the quasi-steady-state nucleation rate.[2,3] However, these rates are not always accessible or they are sometimes difficult to measure.

We present, in this paper, an alternative independent method to determine the free-energy barrier to nucleation of crystallites, directly from their size distributions, independent of any model for W_*, and independent of the energy barrier to the growth. This model-independent method is developed based on our recent results on the dynamic scaling of the cluster size distribution and other universal kinetics in the early stages of nucleation and growth.[4,5] With the temperature dependence of the directly measured W_*, the method also provides the enthalpic and the entropic barriers to the nucleation. The present method is applied to determine the free-energy barrier, the enthalpic, and entropic barriers to the nucleation of the dendritic crystallites observed in the solid-phase crystallization of amorphous Si thin films. Large-grain-sized polycrystalline Si films obtained by crystallizing a-Si films have recently attracted attention, because of their application to the electrical engineering.[6] The applied method provides an opportunity to test the classical model for the free-energy barrier to the nucleation by the directly measured results.

II. METHOD

A. General kinetic basis

Our recent results show that in the early stages of crystallization, the cluster (or crystallite) size distribution (CSD) for sizes within and beyond the nucleation boundary layer obeys dynamic scaling relations.[5] The dynamic scaling relations and their asymptotic limits are invariant to any particular model for W_*. These results not only provide the kinetic basis for the method to measure W_*, using the ratio of the growth rate to the steady-state nucleation rate,[2,3] but also the kinetic basis for the present method based directly on the CSD, as shown in the following.

A proper kinetic description for nucleation and growth[7] was put forwarded based on the general results of the inhomogeneous nonequilibrium processes.[8,9] Let $f(g,t)$ be the actual number concentration of the crystallites consisting of g atoms at a time t, then

$$\frac{\partial f(g,t)}{\partial t} = -\frac{\partial J(g,t)}{\partial g}, \tag{1a}$$

$$J(g,t) = A(g)f(g,t) - D(g)\frac{\partial f(g,t)}{\partial g}, \tag{1b}$$

$$A(g) = \beta(g) - \alpha(g), \tag{1c}$$

$$D(g) = [\beta(g) + \alpha(g)]/2, \tag{1d}$$

where $J(g,t)$ is the flux of the crystallites in the size space, $\beta(g)$ is the addition rate of atoms to a g-sized crystallite, and $\alpha(g)$ is the dissociation rate from a g-sized crystallite. Equation (1) is valid not only for g near the critical size (i.e., in the nucleation barrier layer or the critical region), but also for the observable crystallites much larger than the critical nuclei. Farkas-Becker-Döring-Zeldovich-Frenkel equation[10] that had been conventionally used for describing the nucleation is a special limit of Eq. (1) within the critical region.

The systematic approaches based on boundary-layer theory have been developed for elucidating the dynamic evolution of the CSD within the critical region[11,12] and beyond.[4,5] The results for the dynamic scaling of the CSD beyond the critical region can be transformed into

$$f(g,t) = \eta(g)\frac{\phi(g,t)}{\phi(g,\infty)}, \tag{2}$$

where $\eta(g)$ is the quasi-steady-state distribution, and $\phi(g,t)$ is the transient factor. The transient factor in Eq. (2) is calculated as

$$\phi(g,t) = \mathrm{erfc}\left\{1 + \exp\left[-\frac{t - \lambda\tau - t_g(g_* + \delta, g)}{\tau}\right]\right\} - \mathrm{erfc}\left\{1 + \exp\left[\frac{\lambda\tau + t_g(g_* + \delta, g)}{\tau}\right]\right\}, \tag{3}$$

where g_* is the critical size, δ is the half width of the critical region, $\lambda\tau = -\int_1^{g_*-\delta} dg/A(g)$ is the time to establish the steady state in the subcritical region, $\tau = \delta^2/2\beta(g_*)$ is the time for a near-critical cluster to diffuse across the critical region, and $t_g(g_* + \delta, g) = \int_{g_*+\delta}^{g} dg'/A(g')$ is the time for a stable cluster to grow drifting from the right boundary of the critical region to the g-sized crystallite. The CSD expressed by Eq. (2) is exactly valid as the solution of Eq. (1), for $g \geq g_* + \delta$ and $t > \lambda\tau$.

For large crystallites of $g \gg g_* + \delta$, the probability of growth is much higher than that of decay, therefore, $|\alpha(g)/\beta(g)| \to 0$ or $A(g) \to \beta(g)$. Consequently, we have[13]

$$t_g(g_* + \delta, g) = \int_{g_*+\delta}^{g} \frac{dg'}{\beta(g')}, \tag{4}$$

and

$$\eta(g) = \frac{J_*(t)}{\beta(g)}, \tag{5}$$

with

$$J_*(t) \equiv J(g_*, t) = n_1(t)\exp\left(-\frac{W_*}{kT}\right)\frac{\beta(g_*)}{\sqrt{\pi}\delta}, \tag{6}$$

which is equivalent to the quasi-steady-state nucleation rate.[10,14] Here, $n_1(t)$ is the number concentration of the nucleation site available at a time t, $W_* \equiv W(g_*)$ is the Gibbs free-energy of a critical nucleus, which corresponds to the free-energy barrier to nucleation, k is Boltzmann constant, T is the temperature, and the half width of the critical region is calculated by $\delta = [-W''(g)/2kT]^{-1/2}_{g=g_*}$. Since the crystallites consume the available nucleation sites as they nucleate and grow, $n_1(t)$ decreases with time as $n_1(t) = n_1(0)[1 - \chi(t)]$, where $\chi(t)$ denotes the crystallized volume fraction.

As seen in Eq. (6), W_* is originally included in $J_*(t)$, which also includes $\beta(g_*)$. The addition rate of atoms, $\beta(g)$, is generally proportional to both the activation factor associated with growth and the geometry factor as,

$$\beta(g) \propto \exp(-E_g/kT)\, g^{1-\nu/d}, \tag{7}$$

where E_g is the activation energy to growth or the energy barrier to growth, d is the effective dimension controlling the geometry of the crystallites, and ν is the index that determines the mode of the addition of atoms into crystallites. For the addition mechanism of atoms determined by the chemical reaction at the surface of crystallites, $\nu = 1$, while $\nu = 2$ for the addition limited by the diffusion of atoms. Since the net activation factor in J_* is

$$J_* \propto \exp[-(E_g + W_*)/kT],$$

one cannot separate E_g and W_* only by Arrhenius plots of J_*. The recently introduced method[2,3] solved this problem by using the ratio of the growth rate, U, which is also thermally activated as $U \propto \beta(g) \propto \exp(-E_g/kT)$, to J_*. In the present method, using the CSD, the activation energy to growth, E_g, is automatically canceled in the quasi-steady-state CSD, $\eta(g)$, due to the factor of $\beta(g_*)/\beta(g)$ included.

Thus, for the present method, it is important to extract $\eta(g)$ from the observed $f(g,t)$, which is achieved by the dynamic scaling of the observed CSD with Eqs. (2) and (3). With the value of $\chi(t)$, the g dependence of $\beta(g)$, and the proper estimates of g_* and δ, one can obtain W_* by Eqs. (5) and (6) from just one $\eta(g)$ measured at one temperature and at one time, independent of the barrier to growth included in $\beta(g)$. Moreover, from the temperature dependence of W_* and a basic thermodynamic relationship, the entropic barrier to nucleation, ΔS_*, is obtained by

$$\Delta S_* = -\frac{\partial W_*}{\partial T}. \tag{8}$$

Then the enthalpic barrier to nucleation, ΔH_*, is

$$\Delta H_* = W_* + T\Delta S_*. \tag{9}$$

B. Nucleation of dendritic crystallites in solid-phase crystallization of *a*-Si thin films

The solid-phase crystallization (SPC) of amorphous solids progresses by rearranging the disordered atomic

bonds into the crystalline one, which occurs just at the interface between the crystallites and the surrounding amorphous matrices.[15] There is no long-range transport of atoms that affects the rearrangement. The displacement of the atoms is no more than the bond length. Thus, the addition mechanism of atoms into the crystallites is controlled by the chemical reaction at the interface, and hence, the addition rate is described by

$$\beta(g) = \omega S(g), \tag{10}$$

where ω denotes the addition rate per unit area that contains the activation energy to the growth [i.e., $\omega \propto \exp(-E_g/kT)$], and $S(g)$ is the surface area of crystallites consisting of g atoms. Since ω does not depend on g and $\nu = 1$,

$$S(g) \propto g^{1-1/d}, \tag{11}$$

is predicted from Eq. (7).

The crystallites, which randomly nucleate and grow in the SPC of the a-Si films, do not consist of a perfect single-crystalline domain, but contain numerous twin planes inside. The high-resolution TEM (transmission electron microscope) observation of the annealed films revealed that the crystallites had been multiply twinned, since they were as small as a few nm.[16] The multiple twinning and the crystallographic anisotropy of the growth velocity lead to the dendritic shape of the crystallites.[17] Therefore, the surface area of the dendritic crystallites should be described by a general scaling geometry, rather than the Euclidean one. If the surface area of the crystallites growing in the three-dimensional space is scaling, one may write

$$s_3(r) \propto r^D,$$

where $s_3(r)$ is the measured value of the surface area of the crystallites, whose size is represented by r in a unit of length, and D is the noninteger effective dimension, with respect to r. Provided that the surface of the dendritic crystallites holds a self-similar structure, the surface area is also scaled as[18]

$$s_3(R) \propto R^{-D},$$

where R is a characteristic length scale corresponding to the resolution in the measurement. If r is represented by the effective radius of the crystallites, defining $r(g) \equiv (3v_1 g/4\pi)^{1/3}$, with v_1 being the volume for a single atom, and if R is represented by the curvature, the measured value of the area is exactly expressed as

$$s_3(r, R) = 4\pi r^D R^{2-D}. \tag{12}$$

Although the scaling geometry like $s_3(r, R)$ never attains the actual value, atomic resolution would be virtually adequate to represent $S(g)$ in Eqs. (10) and (11). Taking a limit of $R \to r(1)$, the actual surface area of the dendritic crystallites growing in the three-dimensional space is estimated as

$$\begin{aligned} S_3(r(g)) &= \lim_{R \to r(1)} s_3(r, R) \\ &= 4\pi r^D \left(3v_1/4\pi\right)^{(2-D)/3} = a_3 g^{D/3}, \end{aligned} \tag{13}$$

where $a_3 \equiv (36\pi v_1^2)^{1/3}$. Comparing Eq. (13) with Eq. (11), the relation of $D = 3 - 3/d$ is obtained.

The crystallites growing in thin films eventually reach either the top surface or the bottom surface of the films. They cannot grow freely in the three-dimensional space any longer, but the growth propagates only in the direction of the film plane. Finally, they become the planar dendritic crystallites.[17] Since the origin of a planar crystallites resides within the film, it could be regarded as a thin piece sliced from the three-dimensional dendrite, whose gravity center is also within the film. Therefore, the area of the amorphous-to-crystalline interface is approximately estimated by

$$s_2(r, R) \approx s_3(r, R)\frac{\ell}{2r},$$

where $s_2(r, R)$ is the area of the growing flank of the planar crystallites, ℓ is the film thickness, and r is the effective radius defined by $r(g) = (v_1 g/\pi\ell)^{1/2}$. By the same limitation as in Eq. (13), the actual area of the interface is obtained as

$$\begin{aligned} S_2(r(g)) &= \lim_{R \to r(1)} s_2(r, R) \\ &= 2\pi\ell r^{D-1} \left(v_1/\pi\ell\right)^{-D/2} = a_2 g^{(D-1)/2}, \end{aligned} \tag{14}$$

where $a_2 \equiv 2(\pi v_1 \ell)^{1/2}$.

If the critical nuclei are smaller than the thickness of the a-Si film, the addition rate of atoms into the critical nuclei is

$$\beta(g_*) = \omega S_3(g_*), \tag{15}$$

and if the large and planar crystallites are mainly sampled in the observation of the CSD, the addition rate of atoms into those crystallites is

$$\beta(g) = \omega S_2(g). \tag{16}$$

Substituting Eqs. (13)–(16) into Eq. (5), the quasi-steady-state CSD is obtained as

$$\eta(g) = C g^{1-3/2d}, \tag{17}$$

where

$$C \equiv n_1(t) \exp\left(-\frac{W_*}{kT}\right)\left(\frac{a_3}{a_2}\right)\frac{g_*^{1-1/d}}{\sqrt{\pi\delta}}. \tag{18}$$

On the other hand, substituting Eq. (16) into Eqs. (3) and (4), the transient factors are obtained as

$$\begin{aligned} \phi(g, t) = {} & \operatorname{erfc}\left[1 + \xi\zeta \exp\left(\kappa g^{3/2d}\right)\right] \\ & - \operatorname{erfc}\left[1 + \zeta \exp\left(\kappa g^{3/2d}\right)\right], \end{aligned} \tag{19a}$$

$$\phi(g, \infty) = \operatorname{erfc}[1] - \operatorname{erfc}\left[1 + \zeta \exp\left(\kappa g^{3/2d}\right)\right], \tag{19b}$$

where

$$\xi = \exp(-t/\tau),$$
$$\zeta = \exp(\lambda),$$
$$\kappa = \frac{2d}{3\omega\tau a_2},$$

are the dimensionless parameters.

Using Eq. (18), the free-energy barrier to nucleation is calculated by

$$\frac{W_*}{kT} = -\ln C + \ln\frac{n_1(t)}{\sqrt{\pi}} + \ln\frac{a_3}{a_2} + \ln\frac{g_*^{1-1/d}}{\delta}. \quad (20)$$

The value of C can be determined by the dynamic scaling of the observed CSD with Eqs. (2), (17), and (19). The other terms in the right-hand side of Eq. (20) are known, except for the last one. However, if $\ln[g_*^{1-1/d}/\delta]$ is negligible compared to the others, one can obtain

$$W_* = kT \ln\left[\frac{n_1(t)a_3}{\sqrt{\pi}Ca_2}\right], \quad (21)$$

without invoking any model for W_*. The above approximation will be verified later with the experimental results.

III. EXPERIMENT

A. Sample preparation and data analysis

Amorphous Si films were deposited on the substrates by low-pressure chemical-vapor deposition, using SiH_4 gas at a temperature of 823 K, at a pressure of 40 Pa, and at a rate of 2.8×10^{-5} μm s^{-1}. The substrates were crystalline Si wafers coated by SiO_2 films that were formed as amorphous by thermal oxidation of the wafers. The thickness of the a-Si films was $\ell = 0.1$ μm. Since *in situ* cross-sectional TEM observation has detected a few nm-sized crystallites growing stably,[16] the critical nuclei must be far smaller than the film thickness, and hence, the condition for Eq. (15) is fulfilled. Si^+ ions accelerated to 70 keV were implanted into the a-Si films at room temperature and at the dose of 1×10^{15} cm^{-2}. The implantation of Si^+ ions prior to the annealing reduces the nucleation rate,[19] so as to make the observation easier and more precise. Characterization of these a-Si films has been reported in detail elsewhere.[19] Since those amorphous films are as dense as single-crystalline Si, $v_1 = 2.02 \times 10^{-11}$ μm^3. If all the atoms in the film provide the nucleation site, the density of the nucleation sites projected onto the film plane is estimated as $n_1(0) = 4.96 \times 10^9$ μm^{-2}.

Isothermal annealing in nitrogen ambient induced the spontaneous nucleation of the crystallites and their growth. Table I summarizes the experimental conditions for the four kinds of the samples annealed at 863–893 K. Since the starting amorphous films were crystallite free,[19] and the crystallization hardly occurs at room temperature, the annealing duration directly corresponds to t in $f(g,t)$. The annealing durations were chosen so as to obtain the partially [$\chi(t) \sim 0.1$] crystallized films, in which the coalescence among the adjacent crystallites had scarcely begun.

The annealed films were observed by TEM from the direction normal to the film plane. The plan-view TEM images were analyzed by an image processor to measure the projected area of each crystallite, a_p, the projected perimeter of each crystallite, the maximum length of each crystallite, and the crystalline area fraction of the image fields. The resolution in digitizing the plan-view images was 0.02 μm for both directions in the film plane. A number of the images taken from different parts of the film were used to sample over one thousand crystallites from one sample. The effective radii of the dendritic crystallites were calculated by $r = \sqrt{a_p/\pi}$. The number of atoms contained in a crystallite was estimated by $g = a_p\ell/v_1$. The crystalline area fraction was regarded as equivalent to the crystallized volume fraction, $\chi(t)$.

The perimeter also scales with the crystallite size, due to the dendritic shapes of the crystallites. Assuming that the difference in the effective dimensions between the surface area of the three-dimensional dendrite and the perimeter of its cross section is identical to the difference in their topological dimensions, the measured value of the perimeter is described as

$$p(r,R) = 2\pi r^{D-1}R^{2-D} = p_0 g^{(D-1)/2}, \quad (22)$$

where $p_0 \equiv 2\pi R^{2-D}(v_1/\pi\ell)^{(D-1)/2}$. Thus, the effective dimension of the surface area of the dendrites can be estimated by finding the power-law correlation between

TABLE I. The experimental conditions of the samples and the results of the analysis.

					Fitting parameters			
Label	T (K)[a]	t (s)[b]	$\chi(t)$[c]	d[d]	C (μm^{-2})	ξ	ζ	κ
(a)	863	1.80×10^5	0.120	3.46	4.30×10^{-5}	0.121	3.55	4.13×10^{-5}
(b)	873	1.08×10^5	0.110	3.45	5.34×10^{-5}	0.130	3.62	3.78×10^{-5}
(c)	881	5.40×10^4	0.105	3.47	6.37×10^{-5}	0.133	3.40	4.50×10^{-5}
(d)	893	3.60×10^4	0.115	3.42	7.73×10^{-5}	0.125	3.50	4.32×10^{-5}

[a]Annealing temperature of the a-Si film.
[b]Annealing duration of the a-Si film.
[c]Crystallized volume fraction directly measured in the image processing.
[d]Effective dimension of the surface area of the crystallites determined by the perimeter.

the size and the perimeter.

The size distributions were statistically measured by counting the number concentration of crystallites, whose sizes are within an interval of Δg around g. The number concentration directly obtained is related to the actual $f(g,t)$ by

$$n(g,\Delta g,t)=\int_{g-\Delta g/2}^{g+\Delta g/2} f(g',t)dg' \approx f(g,t)\Delta g, \quad (23)$$

if $|\partial f/\partial g|\,\Delta g \ll 1$. The size-dependent interval was adopted to keep the accuracy almost constant in the observed range of the size. We considered that the small crystallites, whose maximum length was shorter than the film thickness, have not reached the film surface yet. They were eliminated from the CSD to be analyzed, because they did not satisfy the condition to employ Eq. (16).

The dynamic scaling of the CSD was performed by numerically fitting Eqs. (2), (17), and (19) to the observed $f(g,t)$, regarding C, ξ, ζ, and κ as the unknown fitting parameters. The effective dimension predetermined by the perimeter was substituted into the above equations in the fitting. The fitted values of C were used to determine W_* by Eq. (21). With the temperature dependence of W_*, the entropic barrier and the enthalpic barrier to nucleation were measured by applying Eqs. (8) and (9). As a by-product of the method, the addition rate, ω, was also determined using the set of d, ξ, and κ. The activation energy to growth, E_g, was measured by the Arrhenius plot of ω.

B. Experimental results

Figure 1 shows a bright-field image of the plan-view TEM micrographs of the a-Si film that has been annealed at 893 K for 3.6×10^4 s. The dendritic crystallites with distinctive contrast are seen sparsely at random positions in the gray amorphous background. Their size seems to be widely distributed. The film is partially crystallized at $\chi(t)\sim0.115$. The intricate contours of the crystallites can be also observed.

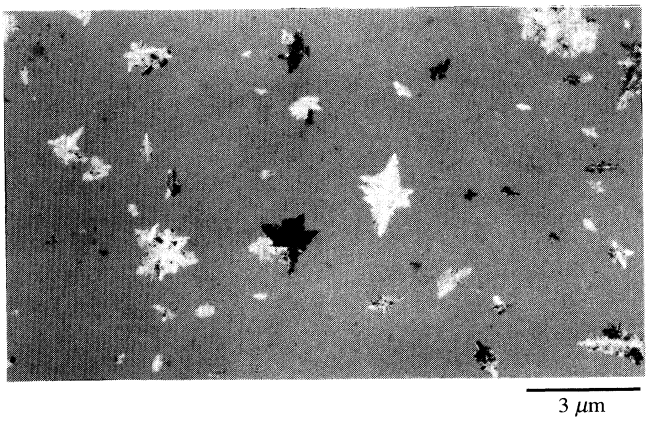

FIG. 1. A bright-field image of the plan-view TEM micrographs of the sample (d) (see Table I). Dendritic crystallites with distinctive contrast are seen sparsely at random positions in the gray amorphous background. The size of the crystallites seems to be widely distributed. The crystallized volume fraction is $\chi(t)=0.115$.

Figure 2 presents the correlation between the size and the measured perimeter, which consists of 1585 crystallites observed in the sample shown in Fig. 1. The top and bottom horizontal axes denote the size represented by the effective radius and the size represented by the number of atoms, respectively. For the tiny crystallites that have not reached the film surface, g in Fig. 2 is not equivalent to the actual number of atoms contained in the crystallites, but only represents their projected size, because it was calculated by $g=\pi r^2\ell/v_1$. However, thus derived g is effective in finding the correlations, using Eq. (22). Each small dot in the plot corresponds to a sampled crystallite. The plot shows an apparent power-law correlation throughout the observed range. The solid line indicates a power function fitted to the data, which is expressed as $p(g)=1.69\times10^{-5}g^{0.562}$ μm. Comparing $p(g)$ to Eq. (22), we obtain the effective dimension by $(D-1)/2=1-3/2d=0.562$. The dashed line represents the size dependence of the circumference of perfect circles expressed by $2\pi r=2\sqrt{\pi v_1 g/\ell}$, which is apparently different from the solid one. With the preexponent of the determined $p(g)$, $R=0.05$ μm is estimated by Eq. (22), which corresponds to the intersection point of the two lines.

Figure 3 shows the CSD observed in the sample of Figs. 1 and 2. The dots in the plot denote $f(g,t)$ per unit area normalized by the process of Eq. (23). The CSD

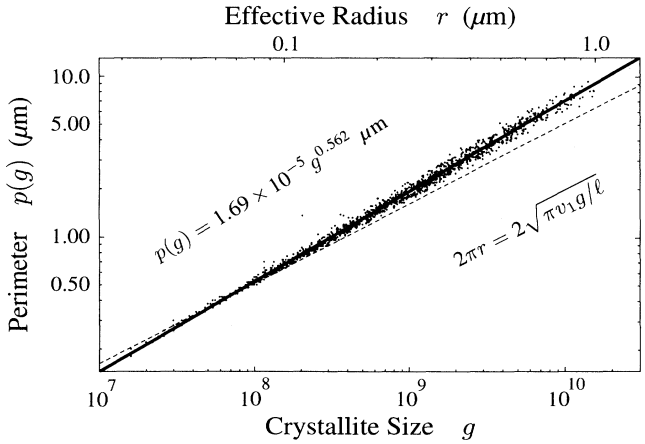

FIG. 2. Correlation between the size and the perimeter observed in the sample (d) (see Table I). The top and bottom horizontal axes denote the size represented by the effective radius, r, and the size represented by the number of atoms, g, respectively. Each small dot in the plot corresponds to a sampled crystallite. The solid line indicates the fitted power function expressed by $p(g)$ printed. The dashed line represents the size dependence of the circumference of perfect circles expressed by $2\pi r$.

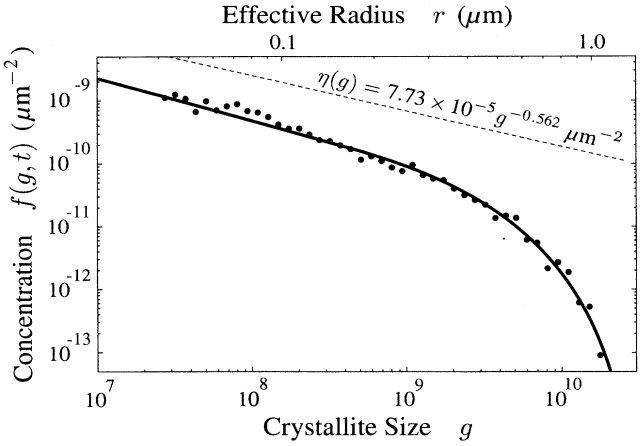

FIG. 3. Crystallite size distribution observed in the sample (d) (see Table I). The horizontal axes are the same of those in Fig. 2. The dots in the plot denote $f(g,t)$ per unit area normalized by the process of Eq. (23). The solid curve indicates $f(g,t)$ fitted to the data. The fitting parameters determined are listed in Table I. The dashed line represents the quasi-steady-state CSD extrapolated by $\eta(g)$ printed. The asymptotic behavior of $f(g,t)$ to the slope of $\eta(g)$ and the rapid drop at $g > 10^9$ are observed.

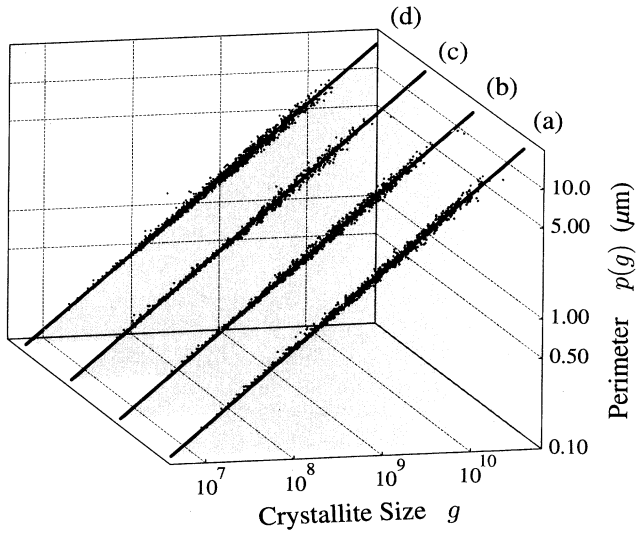

FIG. 4. Correlations between the size and the perimeter observed in the samples (a)–(d) that were annealed at the different temperatures (see Table I). Each small dot in the plot corresponds to a sampled crystallite. The solid lines indicate the fitted power functions. The results of the fitting are listed in Table I.

basically exhibits a monotonous decrease with g, though a rapid drop is also observed in the larger size. The solid curve indicates $f(g,t)$ of Eqs. (2), (17), and (19) that was fitted to the data. We obtained $C = 7.73 \times 10^{-5}$ μm^{-2}, $\xi = 0.125$, $\zeta = 3.50$, and $\kappa = 4.32 \times 10^{-5}$ by the fitting. With the value of C, $W_* = 2.18$ eV is determined by Eq. (21). The dashed line represents the quasi-steady-state CSD extrapolated by $\eta(g)$ of Eq. (17), with the determined values of d and C. Though the observed CSD exhibits the asymptotic behavior to the slope of $\eta(g)$ as g decreases, a considerable difference remains even at the smallest sampling size. This fact means that the CSD in the observed range of size has still been in the transient state.

The stacked plots labeled (a)–(d) in Fig. 4 display the correlations between the size and the perimeter, for the samples annealed at 863, 873, 881, and 893 K, respectively. Figure 5 shows the corresponding stacked plots of the CSD's at those temperatures. The plots labeled (d) are identical with those shown in Figs. 2 and 3. The basic feature of the plots for the samples (a)–(c) are similar to that for the sample (d). It is observed in Fig. 5, however, that the asymptotic limit of $f(g,t)$ slightly increases with the temperature, which reflects the increase of C. Their experimental conditions and the results of the analysis are listed in Table I.

Figure 6 shows the temperature dependence of the free-energy barrier to nucleation, which was determined from C listed in Table I. It appears that W_* linearly increases with the temperature, at least within the observed range of the temperature. Approximating the temperature dependence by the linear function, we obtain $\Delta H_* = 1.32$ eV and $\Delta S_* = -9.57 \times 10^{-4}$ eV K^{-1}.

Figure 7 shows the Arrhenius plot of the addition rates of atoms per unit area that were determined by the fitted parameters listed in Table I. By the slope of the plot, the activation energy to growth was determined as $E_g = 3.42$ eV.

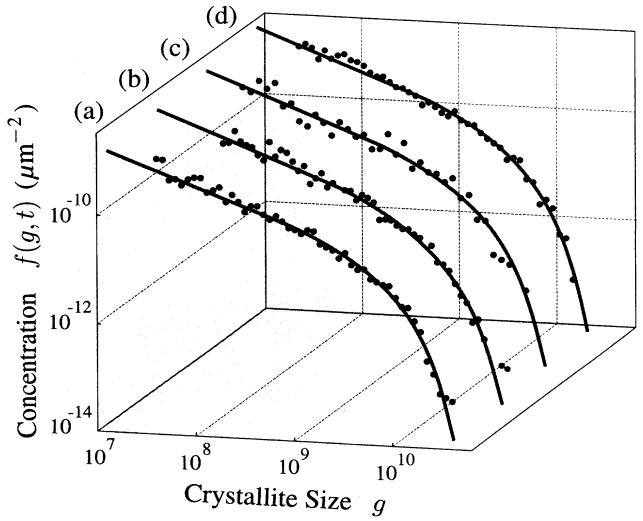

FIG. 5. Crystallite size distributions observed in the samples (a)–(d) that were annealed at the different temperatures (see Table I). The dots in the plot denote $f(g,t)$ per unit area normalized by the process of Eq. (23). The solid curves indicate $f(g,t)$ fitted to the data. The results of the fitting are listed in Table I.

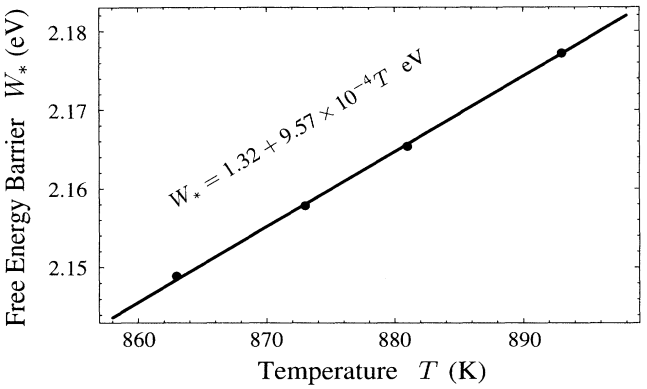

FIG. 6. Temperature dependence of the free-energy barrier to nucleation, W_*. The solid line indicates the fitted linear function expressed by the printed equation. $\Delta H_* = 1.32$ eV and $\Delta S_* = -9.57 \times 10^{-4}$ eV K^{-1} are obtained.

IV. DISCUSSION

A. Method and analysis

As shown in Fig. 2, it is evident that one can never substitute any simple figures (like a circle) for the dendritic crystallites in describing their perimeter. The characteristic length scale in the measurement of the perimeter originates in various experimental factors, such as the original resolution of the TEM micrographs, the reduction of the resolution in digitizing the TEM images, the rounding effect in extracting the edges of the crystallites, and so on. It is reasonable that the estimate of $R = 0.05$ μm is comparable to and greater than the digitizing pixel size of 0.02 μm, which is only one resolution quantitatively prescribed.

If one only glances at the shapes of the observed CSD's in Fig. 5, it may appear as if there is a power-law range

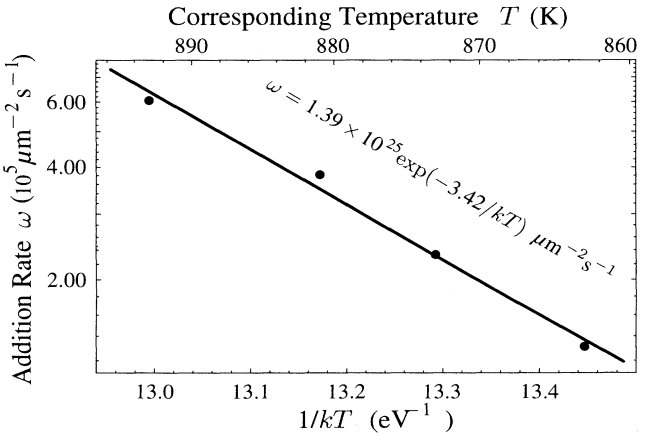

FIG. 7. Arrhenius plot of the addition rates of atoms per unit area, ω. The solid line indicates the fitted exponential function expressed by the printed equation. The activation energy to growth, E_g, is estimated to be 3.42 eV.

in the smaller size ($g < 10^9$). However, as shown in Fig. 2, the comparison with the extrapolated quasi-steady-state CSD revealed that the steady state had not been established in the observed range of the crystallite size. If we mistakenly regarded the pseudo-power-law range as the quasi-steady-state CSD, and besides, directly fitted $\eta(g)$ of Eq. (17) to the selected range without fixing the value of d, we must have obtained a quite different set of d and C. Therefore, without the dynamic scaling by Eq. (2), no one could extract the correct $\eta(g)$ from the transient CSD. It is also important to predetermine the effective dimension, in order to accomplish the correct dynamic scaling of the CSD.

For the purpose of determining W_* by the present method, we need only the value of C. However, the other unknown parameters are also determined in the numerical fitting for the dynamic scaling. The addition rates in Fig. 7 show one of their uses. While more detailed analyses are necessary to fully utilize them, some of the others provide useful information on the validity of the method. For instance, from the values of ξ and ζ determined for the sample (d), we can estimate $\tau = 1.73 \times 10^4$ s and $\lambda = 1.25$. These values indicate that the steady state has already been established beyond the critical region when the CSD was observed at $t = 3.6 \times 10^4$ s, while the observed range was still in the transient state. This situation is common to all the other samples. Thus, the conditions of $t > \lambda\tau$ and $g \geq g_* + \delta$ for Eq. (2) were satisfied.

Now we assess the magnitude of the term $g_*^{1-1/d}/\delta$, which was expected to be negligible. For this purpose, we may simply use the conventional model,

$$W(g) = -g\Delta\mu + \sigma a_3 g^{1-1/d}, \tag{24}$$

where $\Delta\mu$ is the difference in the free energy per atom between the amorphous phase and the crystalline phase, σ is the interfacial-energy density between the crystallite and the amorphous matrix. Using Eq. (24), one has

$$\frac{g_*^{1-1/d}}{\delta} = g_*^{1/2-1/d}\sqrt{\frac{\Delta\mu}{2dkT}}.$$

With $\Delta\mu \approx 0.1$ eV obtained by the calorimetric measurement in the solid-phase epitaxy,[20] the magnitude of the above $g_*^{1-1/d}/\delta$ is estimated at about 0.8–1.5, for the wide variation of g_* from a few tens to hundreds, for the determined values of d, and for the observed range of the temperature. Therefore, $\ln[g_*^{1-1/d}/\delta] \approx -0.3$–$0.5$ can be neglected in Eq. (20), compared to the other terms such as $-\ln C + \ln[n_1(t)/\sqrt{\pi}] \approx 31.2$–$31.8$, and $\ln[a_3/a_2] = 5.57$. The derivative of $\ln[g_*^{1-1/d}/\delta]$ to the temperature is estimated to be about 10^{-5}, which can be also neglected compared with the observed derivative of W_*.

B. Nucleation in SPC of *a*-Si thin films

The free-energy barrier to nucleation in the thermally induced SPC has been measured also by the alternative

method using the ratio of U/J_* for the various a-Si thin films.[3] The values of W_* determined in the present work are close to but slightly greater than that alternative measurement of $W_* \approx 2.0$–2.1 eV. Since both methods have the same kinetic basis, the observed difference of W_* between them could result from either the difference in the starting materials or the difference in the data sources. On the other hand, the present activation energy to growth measured as 3.42 eV is close to those measured by the previous methods.[21,22] The fact that W_* is significantly smaller than E_g shows that the observable rate of nucleation is controlled mainly by the growth of the crystallites rather than the nucleation barrier itself.

Although the temperature range is not sufficiently wide, the directly measured W_* exhibits the apparent temperature dependence. It is remarkable that the entropic contribution (i.e., $-T\Delta S_*$) to W_* is considerably large. This fact suggests that the conventional Arrhenius method for obtaining W_* is not applicable to the present system, because the Arrhenius method equates ΔH_* to W_*.[2] The large entropic contribution to W_* has been found also in a recent study on the nucleation of crystallites in amorphous $CoSi_2$ thin films[23] that uses the alternative U/J_* method. Since the entropic contribution corresponds to the difference in ordering between the amorphous and the crystalline structures, these results indicate that the topological rearrangement of the disordered amorphous structure into the ordered crystalline structure is a process essential to the nucleation event as well as the growth. It is difficult, however, to further discuss at the present stage the origin of the observed large entropic contribution to W_*, because of lack of the more detailed atomistic understanding.

It should be emphasized that the present method for experimentally determining W_* is independent of any model for W_*. Conversely, the obtained results can be used to test the various models for W_*. As the initial trial, we compare the magnitude of W_* estimated from the classical capillary theory with the present result. Using Eq. (24) with $\Delta\mu = 0.1$ eV and $\sigma = 0.310\ \mathrm{Jm^{-2}} = 1.93 \times 10^6\ \mathrm{eV}\mu\mathrm{m}^{-2}$,[24] the classical theory gives $W_* = 9.50$ eV. This is considerably greater than the present experimental determination. It is possible to doubt the use of the above parameters, since they were measured or theoretically estimated not for the small clusters, but for the bulk materials. However, for example, the other reports on σ measured for the small Si crystallites, using the classical theory, give much larger estimates of σ,[25,26] which further raise the magnitude of W_* based on classical model for W_*. Although in the other systems, the experiments and/or the computer simulation have partly supported the classical model,[1,27] we would rather suggest that the classical capillary theory is not applicable to the present system. A recent theory predicts the lowering the nucleation free-energy barrier compared to the classical capillary theory, which is mainly due to the reduction of the interfacial-energy term in the small clusters.[28] The next challenge will be to test such nonclassical models by the directly measured results, including ΔH_* and ΔS_*.

V. CONCLUSION

In conclusion, a method has been introduced to measure the free-energy barrier, W_*, to the nucleation of crystallites directly from their size distributions, independent of any model for W_*, and independent of the energy barrier to the growth. This model-independent method has been developed based on our recent results on the dynamic scaling of the cluster size distribution and other universal kinetic laws in the early stages of nucleation and growth. The method has been applied to determine W_* of dendritic Si crystallites in a-Si thin films. Considering the dendritic nature of the crystallites, we have obtained $W_* \approx 2.15$–2.18 eV, the enthalpic (i.e., the activation energy) barrier $\Delta H_* = 1.32$ eV, the entropic barrier $\Delta S_* = -9.57 \times 10^{-4}\ \mathrm{eV\,K^{-1}}$, within the temperature range of $T = 863$–893 K. It is found that the entropic contribution to W_* is considerably large. In addition, we have shown that the magnitude of the measured W_* could not be accounted for by the classical model for W_* with the previous suggested values for its parameters. Thus, the results obtained by the present model-independent method provide an opportunity for the testing of the various theoretical models for W_*. Finally, we note that the general concept of the method can be readily applied to the other systems.

ACKNOWLEDGMENTS

We would like to thank Y. Niwa and King-Ning Tu for their encouragement and useful suggestions, and Professor Tu for inviting one of the authors to present a seminar at UCLA on the topic of the present paper. Partial support of this work by NASA through grant NAG8-1082 is also gratefully acknowledged.

* Electronic address: kumomi@chcc.canon.co.jp

[1] For reviews and detailed discussions, see K. Binder and D. Stauffer, Adv. Phys. **25**, 343 (1976); K. Binder, Rep. Prog. Phys. **50**, 783 (1987), Sec. 5; K. F. Kelton, Solid State Phys. **45**, 75 (1991); D. W. Oxtoby, J. Phys. Condens. Matter **4**, 7627 (1992).
[2] F. G. Shi, Scr. Metal. Mater. **31**, 1227 (1994).
[3] F. G. Shi, J. Appl. Phys. **76**, 5149 (1994).
[4] F. G. Shi and J. H. Seinfeld, AIChE J. **40**, 11 (1994).
[5] F. G. Shi and J. H. Seinfeld, Mater. Chem. Phys. **37**, 1 (1994).
[6] For a recent review, see, N. Yamauchi and R. Reif, J. Appl. Phys. **75**, 3235 (1994).
[7] F. G. Shi, Scr. Metal. Mater. **30**, 1195 (1994).
[8] F. G. Shi, Chem. Phys. Lett. **212**, 421 (1993); Phys. Lett. A **183**, 311 (1993).

[9] K. Molmer, J. Phys. B **27**, 1889 (1994).
[10] J. Frenkel, *Kinetic Theory of Liquids* (Oxford University Press, Oxford, 1943).
[11] G. Shi, J. H. Seinfeld, and K. Okuyama, Phys. Rev. A **41**, 2101 (1990).
[12] J. J. Hoyt and G. Sunder, Scr. Metal. Mater. **29**, 1535 (1993).
[13] F. G. Shi, Scr. Metal. Mater. **30**, 1151 (1994).
[14] D. Walton, J. Chem. Phys. **37**, 2182 (1962).
[15] T. Saito and I. Ohdomari, Philos. Mag. B **43**, 673 (1981); **49**, 471 (1984).
[16] R. Sinclair, J. Morgiel, A. S. Kirtikar, I. W. Wu, and A. Chiang, Ultramicroscopy **51**, 41 (1993).
[17] T. Noma, T. Yonehara, and H. Kumomi, Appl. Phys. Lett. **59**, 653 (1991).
[18] B. B. Mandelbrot, *Fractals: Form, Chance and Dimension* (Freeman, San Francisco, 1977).
[19] H. Kumomi and T. Yonehara, J. Appl. Phys. **75**, 2884 (1994).
[20] E. P. Donovan, F. Spaepen, D. Turnbull, J. M. Poate, and D. C. Jacobson, J. Appl. Phys. **57**, 1795 (1985).
[21] R. B. Iverson and R. Reif, J. Appl. Phys. **62**, 1675 (1987).
[22] Y. Masaki, P. G. LeComber, and A. G. Fitzgerald, J. Appl. Phys. **74**, 129 (1993), and references therein.
[23] F. G. Shi and K. N. Tu, Phys. Rev. Lett. **74**, 4476 (1995).
[24] F. Spaepen, in *Amorphous Materials: Modeling of Structure and Properties*, edited by V. Vitek (The Metallurgical Society of AIME, New York, 1983), p. 265.
[25] S. Roorda and W. C. Sinke, Appl. Surf. Sci. **36**, 588 (1989).
[26] A. S. Kirtikar, R. Sinclair, J. Morgiel, I.-W. Wu, and A. Chiang, in *Evolution of Thin Film and Surface Microstructure,* edited by C. V. Thompson, J. Y. Tsao, and D. J. Srolovitz, MRS Symposia Proceedings No. 202 (Materials Research Society, Pittsburgh, 1991), p. 627.
[27] K. F. Kelton and A. L. Greer, Phys. Rev. B **38**, 10 089 (1988).
[28] K. K. Mon and D. Jasnow, Phys. Rev. Lett. **59**, 2983 (1987).

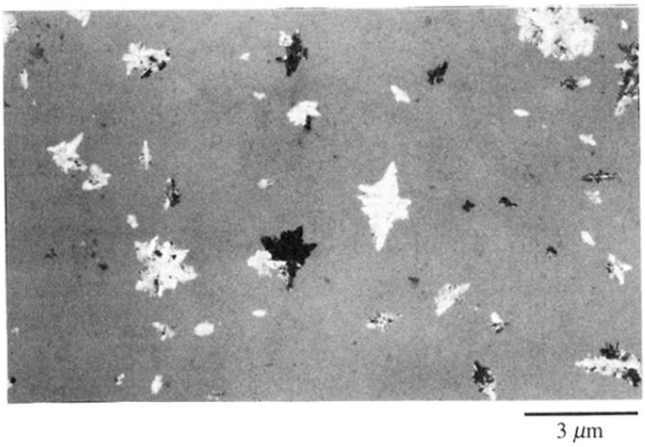

FIG. 1. A bright-field image of the plan-view TEM micrographs of the sample (d) (see Table I). Dendritic crystallites with distinctive contrast are seen sparsely at random positions in the gray amorphous background. The size of the crystallites seems to be widely distributed. The crystallized volume fraction is $\chi(t) = 0.115$.

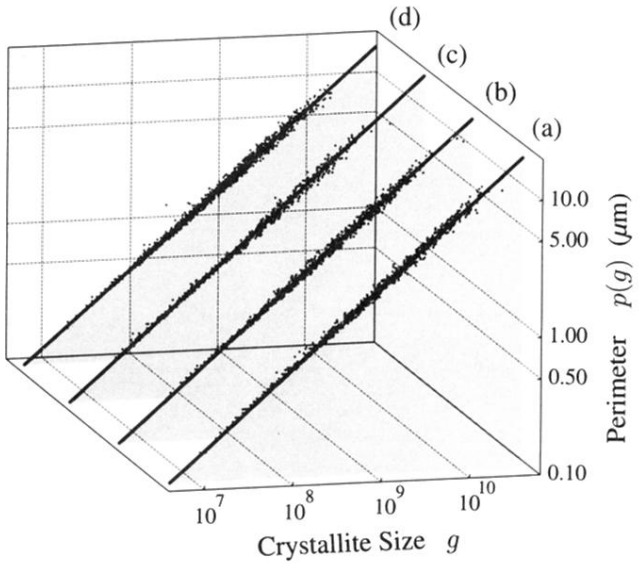

FIG. 4. Correlations between the size and the perimeter observed in the samples (a)–(d) that were annealed at the different temperatures (see Table I). Each small dot in the plot corresponds to a sampled crystallite. The solid lines indicate the fitted power functions. The results of the fitting are listed in Table I.